RESEARCH ARTICLE
ATMOSPHERIC PHYSICS

Earth and Planetary Physics
8: 423–435, 2024
doi: 10.26464/epp2024009

A new electric field mill array with each of the mill's rotor controlled precisely by a GPS module: Equipment and initial results

Kozo Yamashita[1*], Hironobu Fujisaka[2], DaoHong Wang[3], Hiroyuki Iwasaki[4], Kazuo Yamamoto[5], Koichiro Michimoto[6], and Masashi Hayakawa[7]

[1]Department of Production Systems Engineering and Sciences, Komatsu University, Nu 1-3 Shicho-machi, Komatsu, Ishikawa 923-8511, Japan;

[2]Fujisaka Technology Office, 1058-5 Yoshizawa-cho, Ohta-shi, Gunma 373-0019, Japan;

[3]Department of Electrical, Electronic and Computer Engineering, Gifu University, 1-1 Yanagido, Gifu City, Gifu 501-1193, Japan;

[4]Cooperative Faculty of Education, Gunma University, 4-2-Aramaki-machi, Maebashi, Gunma 371-8510, Japan;

[5]Department of Electrical and Electronic Engineering, Chubu University, 1200 Matsumoto-cho, Kasugai, Aichi 487-8501, Japan;

[6]Independent Researcher; Kosenba Town 2-44-11-406, Kawagoe City, Saitama, 350-0036, Japan;

[7]Advanced Wireless & Communications Research Center, The University of Electro-Communications, 1-5-1 Chofugaoka, Chofu, Tokyo 182-8585, Japan

Key Points:

- We have newly designed an electric field mill (EFM) in which the speed and phase of the rotor on each mill has been synchronized within 3% error by using a GPS module, to simplify the estimation of the electric charge transferred by a lightning discharge.
- We deployed five new EFM instruments in the Hokuriku area of Japan during the winter season of 2022–2023 to observe Japanese winter lightning discharges.
- A comparison between the charge positions estimated by our new EFM array and three-dimensional lightning mapping data demonstrates the validity of our methodology.

Citation: Yamashita, K., Fujisaka, H., Wang, D. H., Iwasaki, H., Yamamoto, K., Michimoto, K., and Hayakawa, M. (2024). A new electric field mill array with each of the mill's rotor controlled precisely by a GPS module: Equipment and initial results. *Earth Planet. Phys.*, *8*(2), 423–435. http://doi.org/10.26464/epp2024009

Abstract: We have newly designed an electrostatic sensor, called an electric field mill (EFM), to simplify the estimation of the charge position and charge amount transferred by lightning discharges. It is necessary for this remote estimation of the transferred charge to measure electric field changes caused by charge loss at the time of a lightning strike at multiple locations. For multiple-station measurement of electric field changes, not only speed but also phase for exposure and shielding of the sensing plates inside each EFM of the array should be synchronized to maintain the sensitivities of the deployed instruments. Currently, there is no such EFM with specified speed and phase control performance of the rotary part. Thus, we developed a new EFM in which the rotary mechanism was controlled consistently to within 3% error by a GPS module. Five EFMs had been distributed in the Hokuriku area of Japan during the winter season of 2022–2023 for a test observation. Here we describe the design and a simple calibration method for our new EFM array. Data analysis method based on the assumption of a simple monopole charge structure is also summarized. For validation, locations of assumed point charges were compared with three-dimensional lightning mapping data estimated by radio observations in the MF-HF bands. Initial results indicated the validity to estimate transferred charge amounts and positions of winter cloud-to-ground lightning discharges with our new EFM array.

Keywords: lightning; electrostatic field; electric field mill; electric field change

1. Introduction

There are two main categories for lightning observations. One is to monitor the occurrence of lightning discharges. Electromagnetic fields radiated by a lightning discharge have been measured in various bands to geolocate an individual lightning strike. A two-dimensional (2D) lightning location was estimated based on electromagnetic measurement in wide bands. In the continental United States, more than 100 receivers are distributed to geolocate an individual lightning discharge (Cummins et al., 1998). In Japan, more than 30 receivers are also deployed to monitor lightning activity (Ishii et al., 2005). Measurement in VLF band enables us to monitor the lightning activity on a global scale (Dowden et al., 2002, 2008). Progress in techniques for radio observation makes it possible to estimate three-dimensional (3D) lightning mapping in VHF band (Rison et al., 1999; Zhang GS et al., 2010), MF-HF bands (Ma ZL et al., 2021; Wang DH et al., 2022), and LF band (Yoshida et al., 2014; Wu T et al., 2018; Yuan SF et al. 2020).

Correspondence to: K. Yamashita, kozo.yamashita@komatsu-u.ac.jp
Received 05 OCT 2023; Accepted 28 DEC 2023.
First Published online 06 FEB 2024.

The other purpose is to estimate the electrical properties of a lightning discharge, such as the polarity, peak current, and transferred charge amount. Existing networks for lightning observations provide us with the locations, polarities, and peak currents of individual strikes. In contrast, estimating the charge amount transferred by a lightning discharge is still in the research stage. The transferred charge is an important parameter in lightning risk assessment. A lightning discharge with a huge transferred charge would give rise to heating at the point of a direct lightning strike and cause severe damage. The amount of transferred charge is one of the most essential parameters in determining the level of lightning protection for windmills and tall towers (IEC, 2019; Lightning Risk Management Technology Research Committee for Wind Power Generation Systems, 2019).

The amount of transferred charge is generally estimated in two ways. One is by direct measurement of the lightning current waveforms using a Rogowski coil and a shunt resistor instrumented in or at the foot of a high-rise structure, such as a windmill (Miki et al., 2005; Diendorfer et al., 2009; Ishii et al., 2012; Shindo et al., 2012; Wang XK et al., 2021). The artificial triggering strike current measured by a coaxial shunt also enables us to measure a lightning discharge current directly (Rakov et al., 1998, 2001; Miki et al., 2005; Qie X et al., 2007, 2011; Schoene et al., 2010).

The amount of transferred charge is calculated by integrating the lightning current waveform observed by a Rogowski coil. Direct measurement of the transferred charge has been applied only for direct lightning strikes on high-rise structures. To date, identification of the occurrence of lightning strikes with large amounts of charge has strongly depended on the Rogowski coil system. The frequency distribution for amounts of transferred charges for the full lightning activity has not been derived so far.

The other method is remote estimation of the transferred charge by using electrostatic sensors. Multipoint measurement of electric field changes, which are rapid electrostatic field changes caused by a loss of electric charge resulting from a lightning discharge, is an effective way to derive the magnitudes of transferred charges. Two types of sensors are used to measure electric field changes. One is an electric field mill (EFM), which has popularly been used for electrostatic measurement in atmospheric research. The other is a capacitive sensor, also known as a "slow antenna," which is designed to measure the change in the electric field.

Various designs for an EFM instrument have been proposed in preceding studies (Ogawa, 1973; Chubb, 1990; Bateman et al., 2007; Xu W et al., 2018; Antunes De Sá et al., 2020; Harrison and Marlton, 2020; Agorastou et al., 2022). An essential part of an EFM instrument is the rotary mechanism, which records the strength and direction of the electrostatic field. This rotary mechanism restricts the time resolution of the electrostatic measurement with an EFM. In early research studies for remote estimation of the transferred charge, multipoint measurement of the change in the electric field had been carried out with an EFM network (Jacobson and Krider, 1976; Maier and Krider, 1986). However, it is difficult for an EFM array to measure the change in an electric field, which is recorded as a pulse-shaped waveform on or shorter than the second scale, because of the low time resolution of the EFM. Thus, an EFM has rarely been used to measure the change in an electric field.

In numerous studies, a capacitive sensor, which consists of a sensing plate and a grounded one, had been utilized to estimate the transferred charge (Takeuti et al., 1978; Krehbiel et al., 1979; Brook et al., 1982; Qie X et al., 2000; Cui H et al., 2009; Saito et al., 2009; Zhang TL et al., 2009; Fan XP et al., 2014; Saito, 2016; Kohlmann et al., 2017, 2022; Haley et al., 2021). A capacitive sensor is designed to measure the electric field change to estimate the transferred charge quantitatively and investigate the charge structure inside a thundercloud.

A capacitive sensor offers mainly two advantages in the measurement of an electric field change. The first is that the sampling frequency of a capacitive sensor can be higher than that of an EFM. The sampling frequency for a capacitive sensor can be set high enough to distinguish several signals of electric field changes caused by multiple strikes. The other is that a capacitive sensor has a simple and robust structure, which allows for long-term lightning observations. The maintenance cost for a capacitive sensor is clearly lower than that of an EFM, which has a rotating mechanism that lead to malfunction.

An advantage of the EFM instrument is the simplicity of calibration for sensitivity. The sensitivity of a deployed EFM instrument at each observation site can be evaluated simply by measuring a uniform downward electrostatic field in clear weather, which is called a fair-weather electrostatic field. The strength of a fair-weather electrostatic field varies because of the distortion of electric lines of force. A capacitive sensor is not designed to measure the fair-weather electrostatic field. Measurement of the fair-weather electrostatic field at each observation site is an effective way to compensate for the sensitivities of the distributed EFMs. This methodology would make it easy to select the locations for sensor installations.

However, some technical issues arise when measuring the electric field change by using an EFM array. The time scale of an electric field change is clearly shorter than that of the surface electrostatic field beneath an electrified storm or a fair-weather electrostatic field. It is still difficult for an existing EFM to measure electric field changes because of the insufficient time synchronization of the rotary mechanism inside each EFM, which affects the sensitivities of the deployed instruments.

An EFM consists of a fixed sensing plate and a rotating grounded one. Periodic exposure and shielding of the sensing plate by the rotating grounded plate converts the electrostatic field signal to an alternating current (AC) signal, whose amplitude is recorded as the strength of the electrostatic field. The magnitude of the electric field change is affected by the exposed area of the sensing plate inside the EFM at the moment of a lightning strike. If the exposed areas of the sensing plates in deployed EFMs randomly vary at the time of a lightning discharge, the sensitivities of the deployed EFMs for measuring electric field changes cannot be determined.

The rotation speed of the grounded plate has already been controlled in existing EFM instruments that are used to monitor

electrostatic fields on a scale of minutes associated with thunderstorm activity. However, the variance in the timing for exposure and shielding of the sensing plates inside an individual EFM instrument at each observation has not been discussed in previous studies. Not only the speed but also the timing for exposure and shielding of the sensing plates needs to be controlled to maintain the sensitivities of the distributed EFMs to measure electric field changes. Currently, no such EFM instrument has the specified speed and phase control performance of the rotary part. The development of a new EFM in which the timing for exposure and shielding of the sensing plates are synchronized is a necessary approach to simplify multipoint measurement of electric field changes to estimate the transferred charges.

The objective of this study was to modify an EFM instrument for remote estimation of the transferred charge based on multiple-station measurement of electric field changes. The aim of this improvement was to simplify the methodology used to estimate the positions and amounts of transferred charges. In the new EFM array, both the speed and timing for exposure and shielding of the sensing plates inside each EFM instrument have been controlled consistently to within 3% error by using a GPS module. This new function of the EFM instrument is needed to measure changes in the electric field at multiple points. This modification enables us to realize not only qualitative observation of the electricity inside a thundercloud but also remote estimation of the transferred charge by a lightning discharge with one type of electrostatic sensor.

Five new EFMs were deployed to observe winter lightning unique to the Hokuriku area of Japan during the winter season of 2022–2023 for test observations. We describe the design and calibration method for the new EFM in Section 2. The data analysis method based on the assumption of a simple monopole charge structure is summarized in Section 3. We have derived the locations and amounts of point charges for three lightning discharges. The locations of the assumed point charges were compared with 3D lightning mapping data estimated by radio observations in the MF-HF bands and with 2D lightning location data by electromagnetic measurement in the VLF-LF range. The initial results described in Section 4 indicate the validity of our new EFM array for estimating the charge amounts and positions of winter cloud-to-ground (CG) lightning discharges.

2. Observations

2.1 Instrument

In this study, we originally designed a new EFM for remote estimation of a transferred charge. A schematic diagram of our EFM instrument, which consists of two fixed sensing plates and one rotating grounded plate, is illustrated in Figure 1. A picture of the sensing unit of the developed EFM instrument is shown in Figure 2.

The movement of charge inside an EFM instrument when a positive charge exists above the sensor is shown in Figure 1. If the sensing plates are exposed, a negative charge is induced in the sensing plates because of the downward electrostatic field (Figure 1a). The induced negative charge moves to the ground when the sensing plates are shielded by the grounded plate (Figure 1b). Because of the cyclic shielding and exposure of the sensing plates, the electrostatic field is converted to an AC signal, whose amplitude is recorded as the strength of the measured electrostatic field.

The direction of the electrostatic field on the ground is determined by using the phase of shielding and exposure of the sensing plates. The position of the rotating grounded plate is monitored with a proximity sensor, as shown in Figure 3. The rotation signal level from the proximity sensor becomes high when the rotating grounded plate is positioned above the proximity sensor and the two fixed sensing plates are exposed to the electrostatic field. As described in Figures 1 and 3, a downward electrostatic field leads to electrons from the ground moving to the sensing plates. The rotation signal level becomes low when the rotating grounded plate is not positioned above the proximity sensor and the two fixed sensing plates are shielded. Electrons move from the sensing plates to the ground. If there is an upward electrostatic field, a reverse relationship occurs between the rotation signal from the proximity sensor and the movement of electrons.

Multiple-station measurement of the electric field change fulfills two necessary functions. One is speed control for the rotation of the grounded plate. The period of cyclic exposure of the sensing plates should be constant to maintain the sensitivity of individual sensors. In the case of our developed EFM instrument, the rotation speed was controlled so that the frequency of the rotation signal from a proximity sensor was 10 Hz. This function has been discussed in reports of previous EFM designs (Bateman et al.,

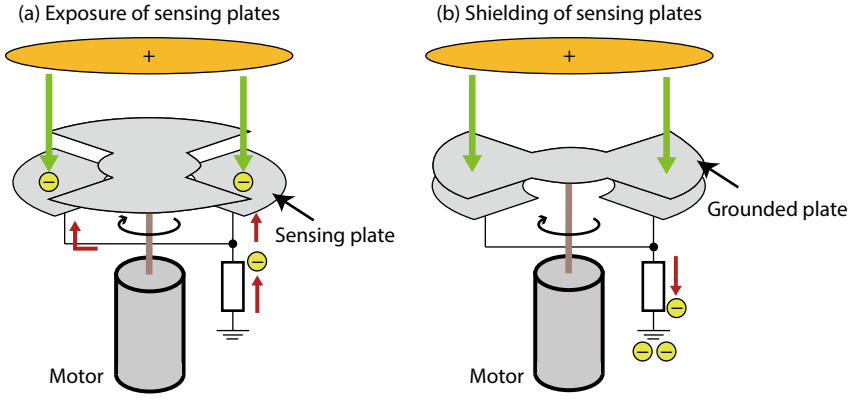

Figure 1. Overview of the EFM.

Figure 2. The sensing unit of our EFM.

2007; Xu W et al., 2018; Antunes De Sá et al., 2020; Harrison and Marlton, 2020).

The other function is synchronization of the periodic shielding and exposure of the sensing plates by the rotation of the grounded plate at multiple locations. The variance of phases for exposure and shielding of the sensing plates cannot be ignored for multipoint measurement of electric field changes, which are rapid changes of the surface electrostatic field. This function has not been discussed in previous studies.

A block diagram of signal processing in the newly developed EFM in this study is shown in Figure 3. The rotation signal from the proximity sensor is compared with a 1 pulse per second (PPS) signal from a global positioning system (GPS) module (GT-902PMGG) with the use of a microcomputer (STM32LK432KC). Not only the rotation speed of the shielding plate but also the timing for shielding and exposure of the sensing plates are synchronized with the rotation control signal from a microcomputer at each observation site.

Shielding and exposure of the sensing plates converts the electrostatic field to an AC signal, whose frequency is 10 Hz. This 10 Hz signal is amplified with an amplifier circuit whose gain is 40 dB. In Figure 3, the amplified 10 Hz signal is described as a "converted electrostatic signal." The maximum and minimum amplitudes and the timing of the converted electrostatic signal are recorded on a SD card as necessary parameters to determine the strength and direction of the electrostatic field by using a microcomputer (STM32LK432KC). The sampling frequency and resolution of analog–digital conversion (ADC) for the converted electrostatic signal are set at 100 Hz and 16 bits, respectively.

Maximum and minimum amplitudes of the converted electrostatic signal during 1 period (100 ms) are calculated and recorded as the strength of the electrostatic field. Additionally, the timing of maximum and minimum values during 1 period of converted electrostatic signal (100 ms) is recorded to determine the direction of the electrostatic field. For example, when the sensing plates are exposed to a downward electrostatic field, an electric current from the sensing plates to the ground generates the maximum value of the converted electrostatic signal. At that time, the rotation signal level from a proximity sensor is high. If an upward electrostatic field exists, the maximum value of the converted electrostatic signal is detected when the rotation signal level is low. By comparison, between the timing of the maximum or minimum value and the rotation signal level from the proximity sensor, the direction of an electrostatic field can be determined. Therefore, the strength and direction of the electrostatic field are recorded every 100 ms with the developed EFM instrument.

Figure 4 shows waveforms of the 1 PPS signal from a GPS module (red line) and that of the rotation signal from a proximity sensor (blue line). These waveforms were recorded with an oscilloscope whose sampling frequency was set as 1000 Hz. The rotation of the grounded plate was controlled to make the rising edges of the rotation signal match that of the 1 PPS signal based on real-time PI (proportional–integral) control by the microcomputer (STM32L432KC). Matching between the rotation signal from the proximity sensor and the 1 PPS signal from the GPS module was conducted every 1 s.

As shown in Figure 5, the difference between the rising edges of rotation signals and those of the 1 PPS signals was summarized by using waveforms of a rotation signal and 1 PPS, which were recorded for a duration of 1 h. The error for rotation timing of a grounded plate was evaluated to be within 3 ms. One period of the rotation signal was 100 ms, so this result indicated that the error of the measured electric field change attributable to rotation variance was within 3%.

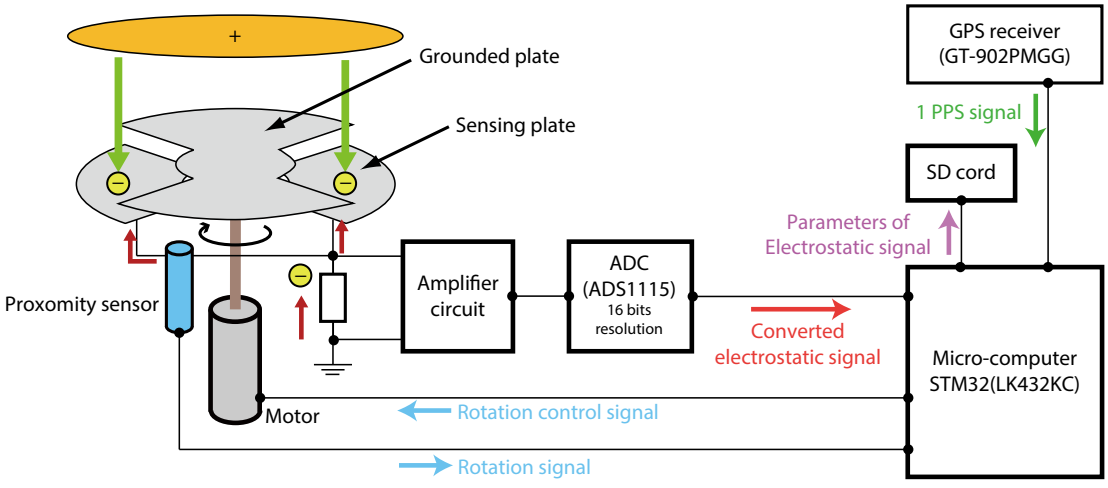

Figure 3. Block diagram of signal processing in the newly developed EFM.

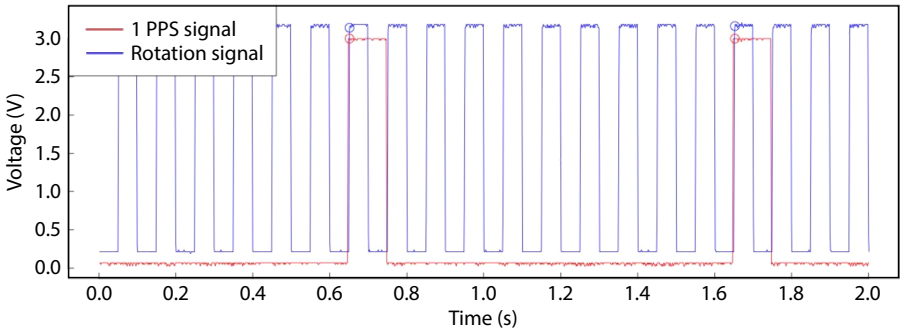

Figure 4. Example of the 1 PPS signal from a GPS module (red line) and that of the rotation signal from a proximity sensor (blue line).

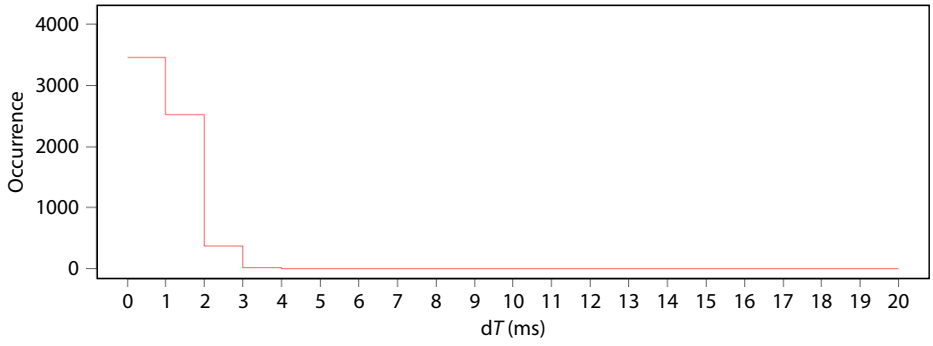

Figure 5. Histogram for the difference between the rising edges of rotation signals and those of the 1 PPS signals.

The specifications for the newly developed EFM instrument described above are summarized in Table 1. The power consumption of the developed system is approximately 1.6 W. All systems are powered by solar power generation systems. We used 50 W solar panels for the power supply to the instrument. This power supply method made it possible to decrease the restrictions on selection of the sensor installation sites, which was a necessary function to simplify the distribution of our developed EFM instruments.

Table 1. Specifications of the developed EFM system.

Parameter	Details
Power-supply voltage	12 V
Power consumption	~1.6 W
Gain of amplifier	40 dB
Analog–digital conversion	0–5000 mV (2450 mV bias), 16 bit resolution
Sampling frequency of the electrostatic field	10 Hz

2.2 Network

Five EFM instruments were deployed in the Hokuriku area in Japan from December 2022 to February 2023. Pictures of the distributed EFM instruments are shown in Figure 6a, and deployment of our new EFM array is summarized in Figure 6b. The EFM instruments were installed at sites 1, 2, 3, 4, and 5 in Figure 6a. The developed EFM instruments were distributed at intervals of approximately 10 km.

The sensing unit of our EFM instrument was placed at a height of approximately 2–3 m above the floor or ground where whole systems were installed. During the winter season in the Hokuriku area in Japan, strong winds often blow. We had experimentally confirmed that the effects of ground particles blown up by the wind could not be ignored if the height of a sensing unit was placed lower than 2 m.

The EFM instrument that was utilized for calibration of our new EFM array was installed at site 0. Details of the calibration are described in Section 2.3. The EFM used for calibration was buried underground, as shown in Figure 6a. The surrounding environment at site 0 is considered flat, and the terrain around the sensors was approximated as an ideal plane. The distortion of electric lines of force at site 0 could be ignored.

2.3 Calibration

The sensitivity of each EFM is affected by the surrounding buildings or landforms. Thus, for electrostatic measurement, it is necessary to correct the distortion in the electric force lines. In this study, the sensitivity of each EFM was evaluated based on simultaneous measurement of the fair-weather electrostatic field (E_{FW}[V/m]), which is a uniform downward electric field that can be observed only in clear weather (Harrison and Nicoll, 2018).

Figure 7a is a schematic diagram of the calibration for the deployed EFMs. In this process, we buried the EFM instrument in the ground and covered it with a metallic plate to measure the fair-weather electrostatic field on the ground (E_{G}[V/m]), whose electric lines of force could not be distorted.

The strength of the fair-weather electrostatic field measured at the *i*th station ($E_{\mathrm{FW}i}$[V/m]) is affected by the surrounding environment and is not equal to that of the uniform downward electric

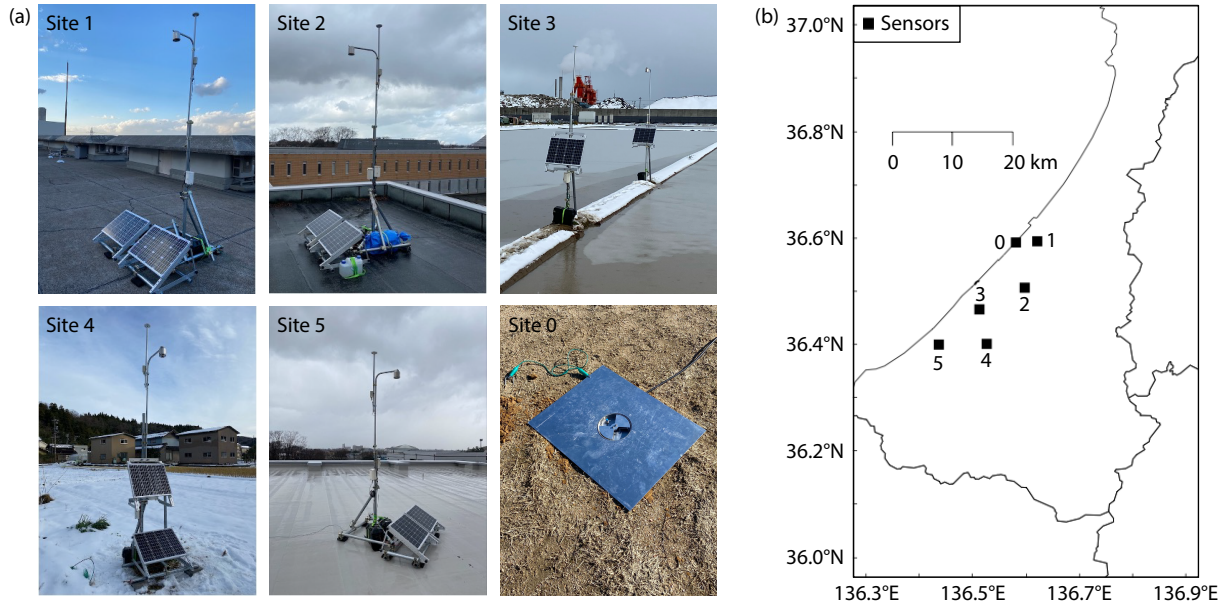

Figure 6. (a) Pictures of the installed sensor systems. (b) Locations of the installed EFMs deployed in the Hokuriku area in Japan during the winter season of 2022–2023.

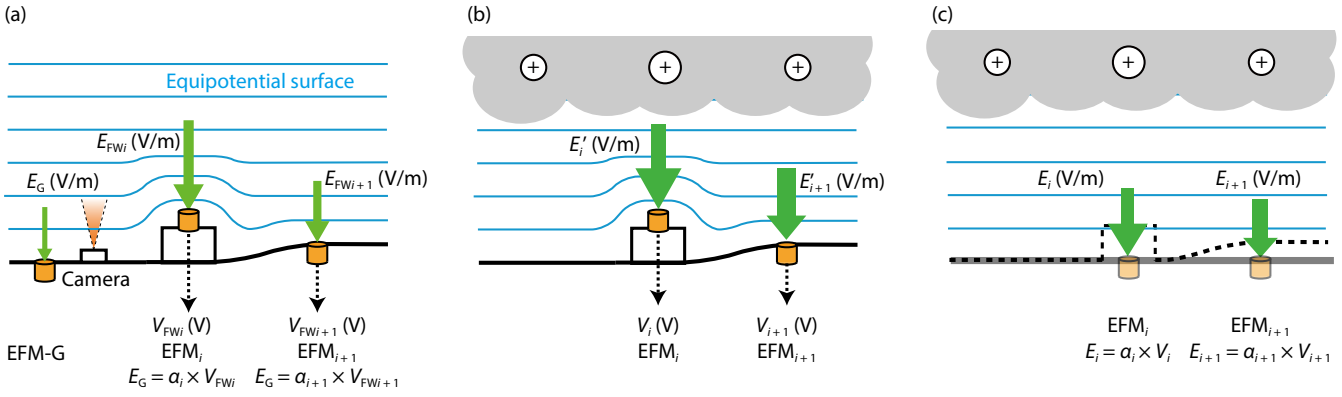

Figure 7. Schematic diagram of calibration for the deployed EFMs. (a) Image for measurement of the fair-weather electrostatic field (E_G[V/m]), which is a uniform downward electric field. Proportional constants (a_i) between the fair-weather electrostatic field (E_G[V/m]) and output voltages from an EFM at the ith site (V_{FWi}[V]) were calculated by using the formula $E_G = a_i \times V_{FWi}$. (b) Image for the electrostatic field beneath an electrified cloud (E_i'[V/m]) at the ith site, which included distorted electric lines of force caused by the surrounding environment and topography. (c) Image for the calibrated electrostatic field (E_i[V/m]) when using proportional constants (a_i) and output voltages from an EFM at the ith site (V_i[V]).

field on the ground (E_G[V/m]) measured at site 0. Fair-weather electrostatic fields (E_{FWi}[V/m]) at the ith station were measured and recorded as an output voltage (V_{FWi}[V]). A proportional constant (a_i) could be calculated by comparing the fair-weather electrostatic field on the ground (E_G[V/m]) at site 0 with the output voltage at the ith site (V_{FWi}[mV]), as described in Figure 7a.

As shown in Figure 7b, electrostatic fields at the ith station (E_i'[V/m]) were recorded as the output voltage from EFM i (V_i[V]) when a thunderstorm passed over the deployed sensors. The surface electrostatic field (E_i'[V/m]) at the ith site included the distortion of electric force lines and was recorded as the output voltage at the ith site (V_i[V]). We multiplied a proportional constant (a_i) and the output voltage at the ith site (V_i[V]) to calculate an electrostatic field whose distortion of electric force lines was corrected (Figure 7c). Example waveforms of output voltages that were coincident with the fair-weather electrostatic field from 11:00 to 12:00 (Japan Standard Time [JST]) on January 11, 2023, are shown in Figure 8. The period of the fair-weather condition was identified by monitoring sky images taken by the camera system. Visual confirmation was also carried out at sites 0, 4, and 5, as described in Figure 7a.

The measured waveform of the fair-weather electrostatic field on the ground (E_G[V/m]) is shown in Figure 8a, and those of output voltages at sites 4 and 5 (V_{FW4}[mV] and V_{FW5}[mV]) are illustrated in Figures 8b and 8c, respectively. The EFM instrument at site 4 was installed on the ground, and that at site 5 was set on the rooftop of a two-story building. Although the fair-weather electrostatic field was simultaneously measured at sites 4 and 5, the output voltage values were different because of distortions of the electric force lines.

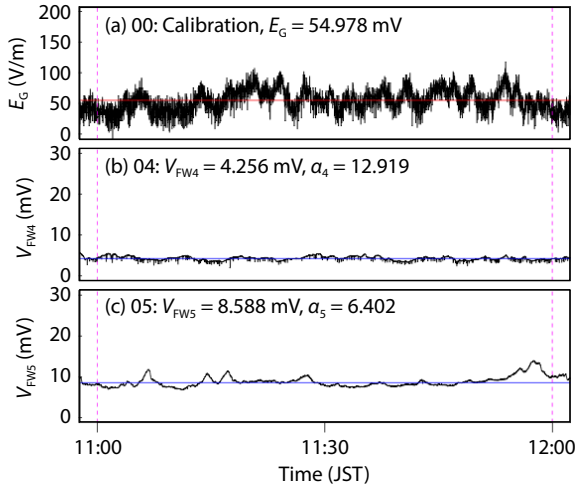

Figure 8. (a) Waveform of the fair-weather electrostatic field (E_G [V/m]) from 11:00 to 12:00 JST on January 11, 2023, measured at site 0. (b, c) Waveforms of the output voltages of our EFM instruments. Our EFMs were installed on the ground at site 4 and on the rooftop of a building at site 5, respectively.

From 11:00 to 12:00 JST on January 11, 2023, average values of the output voltages at sites 4 and 5 were calculated as V_{FW4} = 4.256 mV and V_{FW5} = 8.588 mV. As a result, proportional constants α_4 and α_5 were calculated as 12.92 and 6.402, respectively. We multiplied a proportional constant (α_i) and an output voltage at the ith site (V_i [mV]) to estimate the electric field change, which was to correct a distortion of the electric force lines (E_i [V/m]), as shown in Figure 7c.

3. Data Analysis

3.1 Estimations for Positions and Amounts of Transferred Charges

The positions and amounts of charges transferred by lightning discharges could be calculated by using data on the electric field changes (ΔE[V/m]) measured at multiple locations. In this study, as the structure for the transferred charge, a point charge model was assumed with reference to previous research (Jacobson and Krider, 1976; Krehbiel et al., 1979). The calculated value of the electric field change (ΔE_{ci}[V/m]) at the ith site is described as follows:

$$\Delta E_{ci}(x,y,z,\Delta Q) = \frac{1}{2\pi\epsilon_0}\cdot\frac{\Delta Q\cdot z}{\left\{(x-x_i)^2+(y-y_i)^2+z^2\right\}^{1.5}}, \quad (1)$$

where $\Delta E_{ci}(x,y,z,\Delta Q)$ is in [V/m]. In Equation (1), ΔQ is the amount of electric charge transferred by a lightning discharge.Variables x, y, z are the coordinates of the transferred charge. The locations of the sensors are represented as x_i and y_i. Variable ϵ_0 [F/m] is the dielectric constant in a vacuum. By assuming a simple point charge structure dissipated by a CG lightning discharge, the unknown number is 4. The values of ΔE_{oi}[V/m] measured at more than four sites were required to determine the transferred charge from the position (x,y,z) and amount ΔQ of the CG lightning charge.

The position and amount of a point charge, which are described in Equation (1), were determined by a comparison between the observed value (ΔE_{oi}[V/m]) at each observation site and the theoretical value ($\Delta E_{ci}(x,y,z,\Delta Q)$ [V/m]). To calculate the value of $\Delta E_{ci}(x,y,z,\Delta Q)$ [V/m], the position (x,y,z) and amount ΔQ described in Table 2 were used. The function for determining variables x, y, z and ΔQ is

$$\chi_\nu^2 = \frac{1}{\nu}\sum_{i=1}^{N}\frac{\{\Delta E_{oi}-\Delta E_{ci}(x,y,z,\Delta Q)\}^2}{\sigma_i^2}, \quad (2)$$

where ΔE_{oi}[V/m] is the electric field change measured at the ith station and $\Delta E_{ci}(x,y,z,\Delta Q)$ [V/m] is the theoretical value calculated with Equation (1). Variable ν is the number of degrees of freedom. Variable ν is calculated as the number of sensors minus that of unknowns, and in this work, ν is calculated as 1. Variable σ_i^2 is the variance of the measured ΔE_{oi}[V/m] attributable to observational error. The calibration of EFMs would affect the inaccuracy of magnitudes of the electrostatic field at each site. Errors of the calibrated electrostatic fields at all stations were estimated as less than 10%. In this work, σ_i^2 was defined as 10% of ΔE_{oi}[V/m] measured at the ith station.

We determined the position (x,y,z) and amount (ΔQ[C]) of transferred charge, which minimized the value of χ_ν^2 based on a round-robin calculation using the range of values given in Table 2. In this work, if we found the position and amount that made the minimum value of χ_ν^2 less than 10, the analysis was defined as a success. This criterion was empirically specified.

3.2 Reference Data

For validation, the positions of transferred charges estimated by using the electric field change (ΔE[V/m]) data were compared with two independent types of lightning data. These comparisons were carried out to validate the results of our new EFM array and specify the limitations of the assumed point charge model in this work.

One source was the timing, position, and peak current of lightning discharge data estimated by the Japanese Lightning Detection Network (JLDN). The positions of lightning discharges were compared with those of the transferred charges derived by our

Table 2. Setting of grids (x,y,z) and lightning charge amount ΔQ [C] used to calculate the surface electrostatic field $\Delta E_{ci}(x,y,z,\Delta Q)$ [V/m] at each station.

	Longitude (θ_{ln} [°]), latitude (θ_{lt} [°])	Height (H [m])	Lightning charge amount (ΔQ [C])
Range	$136.1 \le \theta_{ln} \le 136.9$ $36.2 \le \theta_{lt} \le 36.8$	$100 \le H \le 10{,}000$	$1 \le \Delta Q \le 300$
Resolution	0.001°	100 m	1 C

EFM array. In the JLDN dataset, the accuracy of geolocation for a CG and an intracloud (IC) lightning discharge was estimated as 300 m. The detection efficiency of a CG lightning discharge was estimated as more than 90%.

The other source was 3D lightning mapping data based on radio observations. In this work, we referred to 3D lightning mapping data obtained by using an array of discone antennas working in the MF-HF bands. This system is called a discone antenna lightning mapping array (DALMA), and it had been distributed in the same Hokuriku area of Japan for 3D mapping of Japanese winter lightning (Wang DH et al, 2022).

4. Results

As initial results, the charge locations and amounts of three lightning discharges that occurred on December 14, 2022, are summarized in Figures 9, 10, and 11. As described in Section 3, if we found the position and amount that made the minimum value of χ_v^2 less than 10, the analysis was defined as a success in this work. We show Figures 9 and 10 as examples of success and Figure 11 as that of failure.

4.1 Lightning Discharges Observed at 00:48:17 JST on December 14, 2022

In Figures 9(a–e), waveforms of electric field changes (ΔE_{oi}[V/m]) observed at 00:48:17 JST on December 14, 2022, are shown. The horizontal and vertical axes indicate the time and strength of the electrostatic field. Observed values of electric field changes (ΔE_{oi}[V/m]) at the ith site were calculated as the difference between the amplitudes of the surface electrostatic fields described as red circles and those as blue ones in Figures 9(a–e), which represent the values of the surface electrostatic field before and after lightning discharges.

For this event, 1 CG lightning discharge and 2 IC lightning discharges had been detected by the JLDN. The polarity of this CG discharge was negative and its peak current was estimated as −8 kA by the JLDN. The peak current values for the two IC discharges were 9 kA and −7 kA, respectively.

Figures 9f and 9g illustrate plan and height–longitude views of 3D lightning mapping data, JLDN data, and the position of the transferred charge estimated by our EFM array. In Figure 9f, the observation sites are described as black squares, and the numbers of the five sensors are also listed near the black squares filled in. The 3D lightning mapping data derived by the DALMA are described as green scatter dots, and the locations of the CG and IC lightning discharges detected by the JLDN are represented as black square and triangles, respectively. The positions of the assumed point charges are described as red circles in Figures 9f and 9g. Figure 9f demonstrates the agreement between the position of the assumed point charge and those derived by the JLDN and DALMA. This result indicates the validity of the geolocation of the point charge estimated by our EFM array.

Figure 9h is a comparison result between the observed values of electric field changes (ΔE_{oi}[V/m]) at the observation sites and

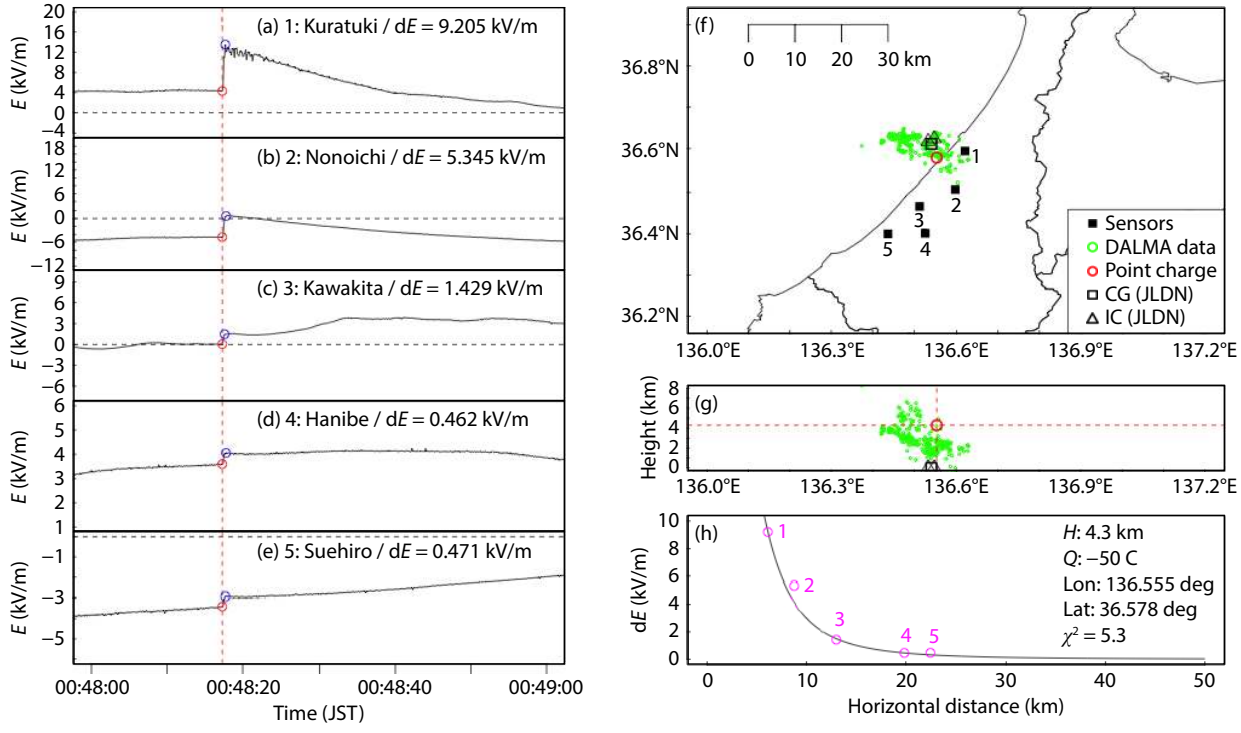

Figure 9. (a–e) Observed waveforms of electric field changes (ΔE_{oi}[V/m]) detected at 00:48:18 JST on December 14, 2022, by using five EFM instruments. The blue circles and red circles in panels (a) to (e) represent the minimum and maximum values of electric field changes (ΔE_{oi}[V/m]). (f) Plan view of 3D lightning mapping data, JLDN data, and estimated position of the transferred charge. (g) Height–longitude view of panel (f). (h) Comparison result between calculated values of electric field changes (ΔE_{ci}[V/m]) with the position and amount of transferred charge that were determined by using Equation (2) and observed values of electric field changes (ΔE_{oi}[V/m]).

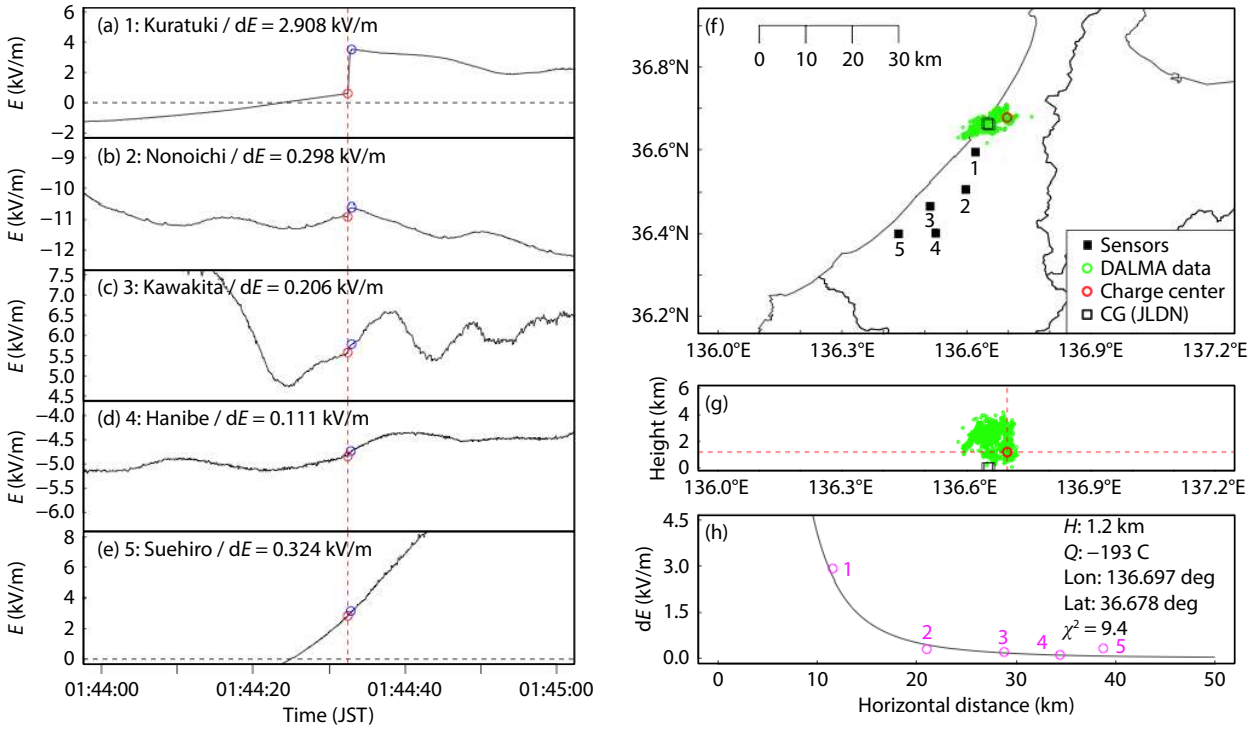

Figure 10. The same as Figure 9 but for the results with waveforms detected at 01:44:32 JST on December 14, 2022.

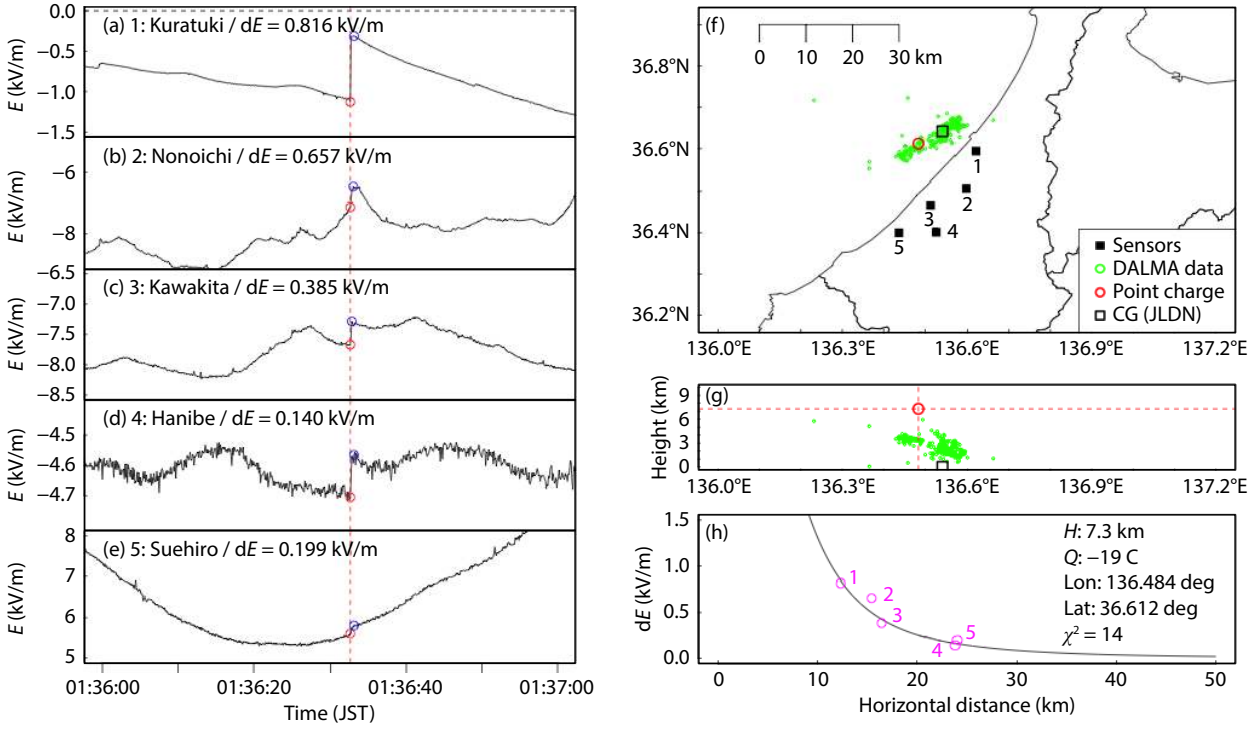

Figure 11. The same as Figure 9 but for the results with waveforms detected at 01:36:32 JST on December 14, 2022.

those calculated ($\Delta E_{ci}(x, y, z, \Delta Q)$ [V/m]) by using Equation (1) with the position (x, y, z) and amount (ΔQ[C]) of transferred charge that minimized the value of χ^2_ν, as described in Equation (2). The horizontal axis refers to the horizontal distance from the estimated location of the transferred charge to the observation sites. The vertical axis indicates the strength of the electric field change. As a criterion for the consistency between the calculated values of ΔE_{ci} and the observed values of ΔE_{oi}, we used the value of χ^2_ν as described in Equation (2). The amount and height of the transferred charge (ΔQ[C]) were calculated as −50 C and 4.3 km, respectively.

In this case, the value of χ^2_ν was calculated as 5.3. This result indicates that the point charge model presumed in this study was suitable as a macroscopic average structure for the charge distri-

bution neutralized by 1 CG and 2 IC discharges. It also demonstrates that the new EFM instruments, in which the speed and phase for exposure and shielding of the sensing plate at each site were synchronized, enabled us to estimate the positions and amounts of transferred charges.

4.2 Lightning Discharges Observed at 01:44:32 JST on December 14, 2022

Observed data at 01:44:32 JST on December 14, 2022, with the same displays as Figure 9, are shown in Figure 10. Two negative CG discharges had been detected by the JLDN. The peak currents were evaluated as −19 kA and −12 kA, respectively. In this case, the value of χ_ν^2 was calculated as 9.4. The amount and height of the transferred charge (ΔQ[C]) were calculated as −193 C and 1.2 km, respectively, by using our EFM array.

In Figures 10f and 10g, the assumed point charges estimated by our EFM array (red circles) were geolocated within the region of DALMA data (green scatter dots). This agreement between the location of the assumed point charge and the distribution of 3D lightning mapping data supports the validity of our methodology.

Additionally, Figure 10 shows the limitations for the electric field change (ΔE_{oi}[V/m]) measurement when using our EFM instruments. If the distance between an observation site and the charge source was more than 30 km, the observed value of ΔE_{oi}[V/m] became too small. In this case, the location and magnitude of the transferred charge was determined based on the observed ΔE_{oi}[V/m] only at sites 1, 2, and 3. The horizontal detection range of our EFM instrument could be estimated as approximately 30 km.

This result provides important information for future expansion of our observation network. In this study, sensors were deployed at intervals of approximately 10 km. To increase the number of observation sites for the multipoint measurement of electric field changes, the density of sensor installation should be high.

4.3 Lightning Discharge Observed at 01:36:32 JST on December 14, 2022

In Figure 11, observed data at 01:36:32 JST on December 14, 2022, are demonstrated with the same displays as Figure 9. In this event, a negative CG discharge had been observed by the JLDN. The peak current of this CG discharge was estimated as −13 kA by the JLDN. The amount and height of the transferred charge (ΔQ[C]) were estimated as −19 C and 7.3 km, respectively, based on our electrostatic measurement.

Figure 11f shows that the longitude and latitude of the assumed point charge (red circle) and JLDN data (black square) were geolocated in the region of DALMA data (green scatter dots). Agreement between the location of the assumed point charge and the distribution of 3D lightning mapping data demonstrates the validity of the methodology developed in this work.

However, the estimated location of the transferred charge (red circle) was different from that of JLDN data (black square) by approximately 10 km horizontally. The JLDN data represents the position of a lightning discharge that was calculated based on measurement of the electromagnetic field radiating from a lightning strike. The location of the assumed point charge shows a macroscopic average center for the charge distribution of the transferred charge. This horizontal 10 km difference between the JLDN data and the assumed point charge could be attributed to the difference in the observation target.

Additionally, in this case, the value of χ_ν^2 was calculated as 14, which exceeded the criterion described above. The DALMA data indicated that the charge structure neutralized by a single CG discharge that occurred at 01:36:32 JST on December 14, 2022, was an elongated charge distribution. These results indicate that the assumed point charge model was not suitable as a macroscopic average structure.

5. Discussion

The aim of this study was to simplify a methodology for estimating the positions and amounts of transferred charges. Multipoint measurement of the electric field change, which is a pulse-shaped waveform on or shorter than the second scale, is needed for remote estimation of the transferred charge. An existing EFM instrument had rarely been utilized to measure electric field changes, although this type of electrostatic sensor could be calibrated simply by measuring the fair-weather electrostatic field. One of the reasons for their limited use was that the deployed EFMs had not been sufficiently synchronized to measure electric field changes at multiple locations.

An EFM has a rotary mechanism, which is required to periodically release the static electricity that accumulates in the device. This rotational part prevents improvements to the accuracy of time synchronization between sensors installed at multiple locations. We made a newly designed EFM instrument in which the speed and phase for exposure and shielding of the sensing plate at each observation site were synchronized to within 3% error by using a GPS module. This function enabled us to synchronize the deployed EFM instruments and maintain their sensitivities for multiple-station measurements of electric field changes.

Five EFMs were distributed in the Hokuriku area of Japan during the winter season of 2022–2023. The deployed EFMs were calibrated by measuring the fair-weather electric field, which could be observed simultaneously at all stations. This calibration method for an EFM included both a sensitivity evaluation of the sensor itself and a sensitivity compensation for the surrounding environment. This simple approach for calibration is an advantage for multipoint measurement of electric field changes when using an EFM array. Three initial results to estimate the locations and amounts of transferred charges based on measurement of the electric field change are shown in Figures 9, 10, and 11.

We had assumed a point charge model as the structure of the transferred charge. The locations of the assumed point charges generally matched the distribution of 3D lightning mapping data estimated by the DALMA. Initial results indicated the possibility of estimating the locations and amounts of transferred charges by using the new EFM array in which the exposure and shielding of sensing plates at each observation site were synchronized.

One of the points to discuss is the value of χ_v^2, which means the agreement between the observed values of electric field changes and the calculated values. A smaller value of χ_v^2 was interpreted as better agreement between the observed and calculated values. The values of χ_v^2 in Figures 9, 10, and 11 were larger than those in previous studies (Jacobson and Krider, 1976; Krehbiel et al., 1979; Brook et al., 1982; Maier and Krider, 1986; Qie X et al., 2000; Cui H et al., 2009; Zhang TL et al., 2009). These results were due to mainly two technical issues.

One issue was the control accuracy of the rotary mechanism inside the new EFM instrument. Currently, exposure and shielding of the sensing plate inside each EFM instrument are synchronized to within 3% error by using the GPS module. The precision for synchronization of the rotating part directly affected the accuracy for multiple-station measurements of electric field changes and the credibility of the transferred charge estimated by the EFM array. Further suppression of control errors for the rotary mechanism is expected to improve the reliability for the position and amount of transferred charge estimated by using the EFM array.

The other issue was the limitation of the assumed point charge structure. Spatial distributions of the DALMA data, as shown in Figures 9, 10, and 11, were clearly different from our point charge model. As shown in Figure 9, 1 CG and 2 IC discharges had been detected at 00:48:18 JST on December 14, 2022. The charge structure neutralized by an IC lightning discharge was a dipole structure. In Figure 11f, the 3D lightning mapping data showed that the charge distribution was of a linear or elliptical shape. The distributions of DALMA data clearly indicate different charge structures from the point charge shapes.

The difference between the actual charge distribution and the assumed point charge model would affect the resulting position and amount of assumed point charge. In this work, we confirmed the impact of the assumed point charge model on the estimated height of the transferred charge. In Figure 9g, the height of the assumed point charge was overestimated as 4.3 km, although the results by the 3D lightning mapping data were mainly distributed over an altitude range of less than 3 km. In Figure 11g, the estimated height of the assumed point charge was overestimated as 7.3 km, although the 3D lightning mapping data were mainly distributed over an altitude range of less than 5 km. The height of the assumed point charge was overestimated by looking at the distribution of DALMA data. This overvaluation would have been caused by a difference between the real charge structure and the assumed point charge model.

These results indicate that the assumption of the point charge model was too simple as a macroscopic average structure of a lightning discharge. In preceding research, a disk charge structure has already been examined (Kohlmann et al., 2022). The scope of application to estimate the transferred charge would be expanded by using a more complex charge model, such as the multiple-point charge model or the disk-shaped charge model.

Extending the charge model to more complex ones would increase the number of distributed sensors, so it would be necessary to increase the number of sensors to be deployed. Initial results demonstrated that the horizontal detection range of our EFM instrument was approximately 30 km. To apply the dipole charge model, it would be preferable for electric field changes to be simultaneously measured at more than eight sites. This means that eight sensors should be deployed within approximately 30 km of the charge source. As shown in Figure 10, the magnitudes of ΔE_{oi}[V/m] at stations more than 30 km away from the charge source were quite low. In this study, sensors had been distributed at intervals of approximately 10 km. To extend the charge model, the interval between each sensor would need to be short to increase the number of sensors for simultaneous measurement of the electric field changes.

Additionally, we should consider the effect of the space charge near the EFM instrument. As mentioned in Section 2.2, we should avoid an effect by ground particles blown up by the wind for electrostatic measurements on the ground. The effect of space charge layers beneath an electrified cloud must also be taken into account (Chauzy and Raizonville, 1982; Chauzy et al., 1991; Qie X et al., 1994). Not only the existence but also the movement of ground surface particles and the space charge layer would act as an error factor for the multiple-station measurement of electric field changes. The verification of error factors is one of the most crucial issues for multipoint measurement of electric field changes. We would need to carry out further data collection for a precise evaluation of the estimated positions and amounts of transferred charges.

6. Conclusions

We deployed five new EFM instruments in the Hokuriku area of Japan during the winter season of 2022–2023 to observe Japanese winter lightning discharges for test observations. An EFM had been newly developed to measure electric field changes at multiple locations for the remote estimation of transferred charges. We had developed an EFM array with each of the mill's rotors controlled consistently within 3% error by using a GPS module. This function was newly designed in this study to maintain the sensitivities of the distributed EFM instruments for multiple-station measurement of electric field changes.

As initial results, three lightning discharges that occurred on December 14, 2022, were analyzed to estimate the locations and amounts of transferred charges. We had assumed a point charge model as the structure of the transferred charge. The calculated locations of the assumed point charges matched the distribution of 3D lightning mapping data estimated by the DALMA. Initial results indicated the possibility that the new EFM array, which had rarely been used to measure electric field changes in previous studies, could be applied to estimate the locations and amounts of transferred charges.

One of the issues encountered was the need to apply a more complex charge model to calculate the locations and amounts of transferred charges. Our initial results suggested that the point charge model was too simple to express the actual structure of a charge neutralized by a winter lightning discharge. In comparison with the 3D lightning mapping data, the height of the assumed point charge was overestimated. It would be difficult to apply this simple charge structure to full lightning discharges. As future work, we would need to consider extending the charge model to

match the assumed charge model with the actual charge distribution.

Acknowledgments

This research is based on results obtained from Project JPNP07015, which was commissioned by the New Energy and Industrial Technology Development Organization (NEDO) and is also partly supported by the Japan Society for the Promotion of Science KAKENHI Program (Grant No. 21K18795). We wish to thank Dr. Minami (Ishikawa Prefectural University), Dr. Funase Dr. Ueda, and Mr. Shibata (Komatsu University) for their grateful support of our observations. We are also grateful to many people at Ishikawa Kenmin Kaihinn Park, Industrial Research Institute of Ishikawa, Ishikawa Prefectural University, Kawakita Farm, Yamashita Farm, and all members at Komatsu University who supported our observations in the winter season of 2022.

References

Agorastou, Z., Noulis, T., and Siskos, S. (2022). Analog sensor interface for field mill sensors in atmospheric applications. *Sensors*, *22*(21), 8405. https://doi.org/10.3390/s22218405

Antunes De Sá, A., Marshall, R., Sousa, A., Viets, A., and Deierling, W. (2020). An array of low-cost, high-speed, autonomous electric field mills for thunderstorm research. *Earth Space Sci.*, *7*(11), e2020EA001309. https://doi.org/10.1029/2020EA001309

Bateman, M. G., Stewart, M. F., Podgorny, S. J., Christian, H. J., Mach, D. M., Blakeslee, R. J., Bailey, J. C., and Daskar, D. (2007). A low-noise, microprocessor-controlled, internally digitizing rotating-vane electric field mill for airborne platforms. *J. Atmos. Oceanic Technol.*, *24*(7), 1245–1255. https://doi.org/10.1175/JTECH2039.1

Brook, M., Nakano, M., Krehbiel, P., and Takeuti, T. (1982). The electrical structure of the Hokuriku winter thunderstorms. *J. Geophys. Res.: Oceans*, *87*(C2), 1207–1215. https://doi.org/10.1029/JC087iC02p01207

Chauzy, S., and Raizonville, P. (1982). Space charge layers created by coronae at ground level below thunderclouds: Measurements and modeling. *J. Geophys. Res.: Oceans*, *84*(C4), 3143–3148. https://doi.org/10.1029/JC087iC04p03143

Chauzy, S., Medale, J. C., Prieur, S., and Soula, S. (1991). Multilevel measurement of the electric field underneath a thundercloud: 1. A new system and the associated data processing. *J. Geophys. Res.: Atmos.*, *96*(D12), 22319–22326. https://doi.org/10.1029/91JD02031

Chubb, J. N. (1990). Two new designs of 'field mill' type fieldmeters not requiring earthing of rotating chopper. *IEEE Trans. Ind. Appl.*, *26*(6), 1178–1181. https://doi.org/10.1109/28.62405

Cui, H., Qie, X., Zhang, Q., Zhang, T., Zhang, G., and Yang, J. (2009). Intracloud discharge and the correlated basic charge structure of a thunderstorm in Zhongchuan, a Chinese inland plateau region. *Atmos. Res.*, *91*(2-4), 425–429. https://doi.org/10.1016/j.atmosres.2008.06.007

Cummins, K. L., Murphy, M. J., Bardo, E. A., Hiscox, W. L., Pyle, R. B., and Pifer, A. E. (1998). A combined TOA/MDF technology upgrade of the U. S. national lightning detection network. *J. Geophys. Res.: Atmos.*, *103*(D9), 9035–9044. https://doi.org/10.1029/98JD00153

Diendorfer, G., Pichler, H., and Mair, M. (2009). Some parameters of negative upward-initiated lightning to the Gaisberg tower (2000–2007). *IEEE Trans. Electromagn. Compat.*, *51*(3), 443–452. https://doi.org/10.1109/TEMC.2009.2021616

Dowden, R. L., Brundell, J. B., and Rodger, C. J. (2002) VLF lightning location by time of group arrival (TOGA) at multiple sites. *J. Atmos. Sol. Terr. Phys.*, *64*, 817–830. https://doi.org/10.1016/S1364-6826(02)00085-8

Dowden, R. L., Holzworth, R. H., Rodger, C. J., Lichtenberger, J., Thomson, N. R., Jacobson, A. R., Lay, E., Brundell, J. B., Lyons, T. J., … Zhao, Y. (2008). World-wide lightning location using VLF propagation in the Earth–ionosphere waveguide. *IEEE Antennas Propag. Mag.*, *50*(5), 40–60. https://doi.org/10.1109/MAP.2008.4674710

Fan, X. P., Zhang, G. S., Wang, Y. H., Li, Y. J., Zhang, T., and Wu, B. (2014). Analyzing the transmission structures of long continuing current processes from negative ground flashes on the Qinghai-Tibetan Plateau. *J. Geophys. Res.: Atmos.*, *119*(5), 2050–2063. https://doi.org/10.1002/2013JD020402

Haley, S., Behnke, S., Edens, H., and Thomas, R. (2021). Observations show charge density of volcanic plumes is higher than thunderstorms. *J. Geophys. Res.: Atmos.*, *126*(19), e2021JD035404. https://doi.org/10.1029/2021JD035404

Harrison, R. G., and Nicoll, K. A. (2018). Fair weather criteria for atmospheric electricity measurements. *J. Atmos. Sol. Terr. Phys.*, *179*, 239–250. https://doi.org/10.1016/j.jastp.2018.07.008

Harrison, R. G., and Marlton, G. J. (2020). Fair weather electric field meter for atmospheric science platforms. *J. Electrost.*, *107*, 103489. https://doi.org/10.1016/j.elstat.2020.103489

IEC. (2019). Wind energy generation systems—Part 24: Lightning protection. (Technical Report IEC 61400-24). Geneva, Switzerland: IEC.

Ishii, M., Saito, M., Fujii, F., Hojo, J. I., Matsui, M., Itamoto, N., and Shinjo, K. (2005). LEMP from lightning discharges observed by JLDN. *IEEJ Trans.*, *125*(8), 765–770. https://doi.org/10.1541/ieejpes.125.765

Ishii, M., Saito, M., Chihara, M., and Natsuno, D. (2012). Transferred charge and specific energy associated with lightning hitting wind turbines in Japan. *IEEJ Trans. Power Energy*, *132*(3), 294–295. https://doi.org/10.1541/ieejpes.132.294

Jacobson, E. A., and Krider, E. P. (1976). Electrostatic field changes produced by Florida lightning. *J. Atmos. Sci.*, *33*(1), 103–117. https://doi.org/10.1175/1520-0469(1976)033

Kohlmann, H., Schulz, W., and Pichler, H. (2017). Compensation of integrator time constants for electric field measurements. *Electr. Power Syst. Res.*, *153*, 38–45. https://doi.org/10.1016/j.epsr.2016.07.014

Kohlmann, H., Schulz, W., and Rachidi, F. (2022). Estimation of charge transfer during long continuing currents in natural downward flashes using single-station E-field measurements. *J. Geophys. Res.: Atmos.*, *127*(6), e2021JD036197. https://doi.org/10.1029/2021JD036197

Krehbiel, P. R., Brook, M., and McCrory, R. A. (1979). An analysis of the charge structure of lightning discharges to ground. *J. Geophys. Res.*, *84*(C5), 2432–2456. https://doi.org/10.1029/JC084iC05p02432

Lightning Risk Management Technology Research Committee for Wind Power Generation Systems. (2019). In recent trends suggestions lightning risk manage wind power system. Technical report for the Institute of Electrical Engineers of Japan, Number 1422. Tokyo, Japan: IEEJ Electronic Library, pp. 4–8 (in Japanese).

Ma, Z. L., Jiang, R. B., Qie, X., Xing, H. Y., Liu, M. Y., Sun, Z. L., Qin, Z. L., Zhang, H. B., and Li, X. (2021). A low frequency 3D lightning mapping network in north China. *Atmos. Res.*, *249*, 105314. https://doi.org/10.1016/j.atmosres.2020.105314

Maier, L. M., and Krider, E. P. (1986). The charges that are deposited by cloud-to-ground lightning in Florida. *J. Geophys. Res.*, *91*(D12), 13275–13289. https://doi.org/10.1029/JD091iD12p13275

Miki, M., Rakov, V. A., Shindo, T., Diendorfer, G., Mair, M., Heidler, F., Zischank, W., Uman, M. A., Thottappillil, R., and Wang, D. (2005). Initial stage in lightning initiated from tall objects and in rocket-triggered lightning. *J. Geophys. Res.: Atmos.*, *110*(D2), D02109. https://doi.org/10.1029/2003JD004474

Ogawa, T. (1973). Analyses of measurement techniques of electric fields and currents in the atmosphere. Kyoto: Contributions of the Geophysical Institute, Kyoto University, 13, pp. 111–137.

Qie, X., Soula, S., and Chauzy, S. (1994). Influence of ion attachment on the vertical distribution of the electric field and charge density below a thunderstorm. *Ann. Geophys.*, *12*(12), 1218–1228. https://doi.org/10.1007/s00585-994-1218-6

Qie, X., Yu, Y., Liu, X., Guo, C., Wang, D., Watanabe, T., and Ushio, T. (2000). Charge analysis on lightning discharges to the ground in Chinese inland plateau (close to Tibet). *Ann. Geophys.*, *18*(10), 1340–1348. https://doi.org/

10.1007/s00585-000-1340-z

Qie, X., Zhang, Q. L., Zhou, Y. J., Feng, G. L., Zhang, T. L., Yang, J., Kong, X. Z., Xiao, Q. F., and Wu, S. J. (2007). Artificially triggered lightning and its characteristic discharge parameters in two severe thunderstorms. *Sci. China Ser. D Earth Sci.*, *50*(8), 1241–1250. https://doi.org/10.1007/s11430-007-0064-2

Qie, X., Jiang, R. B., Wang, C. X., Yang, J., Wang, J. F., and Liu, D. X. (2011). Simultaneously measured current, luminosity, and electric field pulses in a rocket-triggered lightning flash. *J. Geophys. Res.: Atmos.*, *116*(D10), D10102. https://doi.org/10.1029/2010JD015331

Rakov, V. A., Uman, M. A., Rambo, K. J., Fernandez, M. I., Fisher, R. J., Schnetzer, G. H., Thottappillil, R., Eybert-Berard, A., Berlandis, J. P., … Bondiou-Clergerie, A. (1998). New insights into lightning processes gained from triggered-lightning experiments in Florida and Alabama. *J. Geophys. Res.: Atmos.*, *103*(D12), 14117–14130. https://doi.org/10.1029/97JD02149

Rakov, V. A., Crawford, D. E., Rambo, K. J., Schnetzer, G. H., Uman, M. A., and Thottappillil, R. (2001). *M*-component mode of charge transfer to ground in lightning discharges. *J. Geophys. Res.: Atmos.*, *106*(D19), 22817–22831. https://doi.org/10.1029/2000JD000243

Rison, W., Thomas, R. J., Krehbiel, P. R., Hamlin, T., and Harlin, J. (1999). A GPS-based three-dimensional lightning mapping system: Initial observations in central New Mexico. *Geophys. Res. Lett.*, *26*(23), 3573–3576. https://doi.org/10.1029/1999GL010856

Saito, M., Ishii, M., Kawamura, H., and Shindo, T. (2009). Location of negative charge associated with continuing current of upward lightning flash in winter. *IEEJ Trans. Power Energy*, *129*(7), 929–934. https://doi.org/10.1541/ieejpes.129.929

Saito, M. (2016). Study on development of advanced LLS (2)—Proposal on estimation method of the lightning charge amount associated with ground flashes. Komae-shi: CRIEPI. (in Japanese)

Schoene, J., Uman, M. A., and Rakov, V. A. (2010). Return stroke peak current versus charge transfer in rocket-triggered lightning. *J. Geophys. Res.: Atmos.*, *115*(D12), D12107. https://doi.org/10.1029/2009JD013066

Shindo, T., Sekioka, S., Ishii, M., Shiraishi, H., and Natsuno, D. (2012). Studies of lightning protection design for wind power generation systems in Japan. Paris: CIGRE.

Takeuti, T., Nakano, M., Brook, M., Raymond, D. J., and Krehbiel, P. (1978). The anomalous winter thunderstorms of the Hokuriku Coast. *J. Geophys. Res.: Oceans*, *83*(C5), 2385–2394. https://doi.org/10.1029/JC083iC05p02385

Wang, D. H., Wu, T., Huang, H. T., Yang, J. C., and Yamamoto, K. (2022). 3D mapping of winter lightning in Japan with an array of Discone Antennas. *IEEJ Trans. Electr. Electron. Eng.*, *17*(11), 1606–1612. https://doi.org/10.1002/tee.23667

Wang, X. K., Wang, D. H., He, J. J., and Takagi, N. (2021). Characteristics of electric currents in upward lightning flashes from a windmill and its lightning protection tower in Japan, 2005–2016. *J. Geophys. Res.: Atmos.*, *126*(8), e2020JD034346. https://doi.org/10.1029/2020JD034346

Wu, T., Wang, D. H., and Takagi, N. (2018). Lightning mapping with an array of fast antennas. *Geophys. Res. Lett.*, *45*(8), 3698–3705. https://doi.org/10.1002/2018GL077628

Xu, W., Zhang, C. C., Ji, X. Y., and Xing, H. Y. (2018). Inversion of a thunderstorm cloud charging model based on a 3D atmospheric electric field. *Appl. Sci.*, *8*(12), 2642. https://doi.org/10.3390/app8122642

Yoshida, S., Wu, T., Ushio, T., Kusunoki, K., and Nakamura, Y. (2014). Initial results of LF sensor network for lightning observation and characteristics of lightning emission in LF band. *J. Geophys. Res.: Atmos.*, *119*(21), 12034–12051. https://doi.org/10.1002/2014JD022065

Yuan, S. F., Qie, X., Jiang, R. B., Wang, D. F., Sun, Z. L., Srivastava, A., and Williams, E. (2020). Origin of an uncommon multiple-stroke positive cloud-to-ground lightning flash with different terminations. *J. Geophys. Res.: Atmos.*, *125*(15), e2019JD032098. https://doi.org/10.1029/2019JD032098

Zhang, G. S., Wang, Y. H., Qie, X., Zhang, T., Zhao, Y. X., Li, Y. J., and Cao, D. J. (2010). Using lightning locating system based on time-of-arrival technique to study three-dimensional lightning discharge processes. *Sci. China Earth Sci.*, *53*(4), 591–602. https://doi.org/10.1007/s11430-009-0116-x

Zhang, T. L., Qie, X., Yuan, T., Zhang, G. S., Zhang, T., and Zhao, Y. (2009). Charge source of cloud-to-ground lightning and charge structure of a typical thunderstorm in the Chinese inland plateau. *Atmos. Res.*, *92*(4), 475–480. https://doi.org/10.1016/j.atmosres.2009.01.020